

Metabolites in Safety Testing (MIST) Assessment in Early Clinical

Development: A Case Study with a Glucokinase Activator

Raman Sharma, John Litchfield, Karen Atkinson, Heather Eng, Neeta B. Amin, William S. Denney, John C. Pettersen, Theunis C. Goosen, Li Di, Esther Lee, Jeffrey A. Pfefferkorn, Deepak K. Dalvie, and Amit S. Kalgutkar

Pfizer Inc., Eastern Point Road, Groton, CT (R.S., K. A., H.E., J.C.P., T. C. G., L. D.) San Diego, CA (D.K.D.) and Cambridge MA (N.B.A., J.L, W.S.D., E.L., J.A.P., A.S.K.)

Running Title: MIST analysis of a glucokinase activator

Address correspondence to: Amit S. Kalgutkar, Pharmacokinetics, Dynamics, and Metabolism-New Chemical Entities, Pfizer Worldwide Research and Development, 610 Main Street, Cambridge, MA 02139, USA. Tel: +(617)-551-3336. E-mail: amit.kalgutkar@pfizer.com

Text Pages (including references): 37

Tables: 3

Figures: 8

References: 28

Abstract: 252

Introduction: 542

Discussion: 1493

Abbreviations used are: T2DM, type 2 diabetes mellitus; GK, glucokinase; PF-04937319, *N,N*-dimethyl-5-((2-methyl-6-((5-methylpyrazin-2-yl)carbamoyl)benzofuran-4-yl)oxy)pyrimidine-2-carboxamide; CYP, cytochrome P450; M1, *N*-methyl-5-((2-methyl-6-((5-methylpyrazin-2-yl)carbamoyl)benzofuran-4-yl)oxy)pyrimidine-2-carboxamide; MIST, Metabolites in Safety Testing; reduced NADPH, β -nicotinamide adenine dinucleotide 2'-phosphate; HLM, human liver microsomes; DMSO, dimethyl sulfoxide; ISEF, intersystem extrapolation factors; LC-MS/MS, liquid chromatography tandem mass spectrometry; CID, collision-induced dissociation; m/z , mass to charge ratio; MH^+ , protonated molecular ion; AUC, area under the plasma concentration-time curve; C_{max} , maximal plasma concentration; T_{max} , time for occurrence of C_{max} ; f_u , unbound fraction; t_R , retention time; NOAEL no-observed-adverse-effect level; $t_{1/2}$, half-life; DDI, drug-drug interaction.

Abstract

The present article summarizes MIST studies on a glucokinase activator PF-04937319, which is under development for the treatment of T2DM. Metabolic profiling in rat, dog and human hepatocytes revealed that PF-04937319 is metabolized via oxidative (major) and hydrolytic pathways (minor). *N*-Demethylation to metabolite M1 was the major metabolic fate of PF-04937319 in human (but not rat or dog) hepatocytes, and was catalyzed by CYP3A and CYP2C isoforms. Qualitative examination of circulating metabolites in humans at the 100 mg and 300 mg doses from a 14-day multiple dose study revealed unchanged parent drug and M1 as principal components. Because M1 accounted for 65% of the drug related material at steady state, an authentic standard was synthesized and used for comparison of steady state exposures in human and the 3-month safety studies in rats and dogs at the NOAEL. Although circulating levels of M1 were very low in beagle dogs and female rats, adequate coverage was obtained in terms of total C_{max} (~7.7x and 1.8x) and AUC (3.6x and 0.8x AUC) relative to the 100 mg and 300 mg, doses, respectively in male rats. Examination of primary pharmacology revealed M1 was less potent as a glucokinase activator than the parent drug (compound PF-04937319:EC₅₀=0.17 μM; M1:EC₅₀=4.69 μM). Furthermore, M1 did not inhibit major human CYP enzymes (IC₅₀>30 μM), was negative in the *Salmonella* Ames assay, with minimal off-target pharmacology, based on CEREP broad ligand profiling. Insights gained from this analysis should lead to a more efficient and focused development plan for fulfilling MIST requirements with PF-04937319.

Introduction

Type 2 diabetes mellitus (T2DM), characterized by elevated levels of fasting blood glucose, is a complex disease mainly caused by defects in hepatic glucose metabolism and the failure of pancreatic β -cells to secrete enough insulin to overcome insulin resistance. Glucokinase (GK) activators offer a novel and promising opportunity for the treatment of T2DM patients (Matschinsky et al., 2011; Sarabu et al., 2011; Pfefferkorn, 2013). GK is a member of hexokinase family of enzymes that are responsible for the phosphorylation of glucose to glucose-6-phosphate (Mithieux, 1996). GK plays a key role in glucose homeostasis by promoting glycogen synthesis in the liver and glucose-sensitive insulin release in β -cells (Matschinsky and Ellerman, 1968; Matschinsky et al., 1998). Activators of GK increase the enzyme's affinity for glucose (K_m) and also its maximal catalytic rate (V_{max}). Consequently, they stimulate insulin biosynthesis and secretion, enhance hepatic glucose uptake, and augment glucose metabolism and related processes in GK-expressing cells. Early clinical studies of GK activators have demonstrated improvements in glycemic control, in both healthy volunteers and T2DM patients (Haynes et al., 2010; Coghlan and Leighton, 2008; Meininger et al., 2011; Sarabu et al., 2012); however, an elevated risk of hypoglycemia arising from GK activation in the pancreas leading to inappropriately excessive insulin secretion was also observed. Medicinal chemistry strategies to overcome the hurdles imposed by the hypoglycemia risk have been recently reviewed (Pfefferkorn, 2013). One such tactic involves the design of "partial activators" of GK that avoid reducing the K_m for glucose to inappropriately low levels, thereby retaining increased dependence of enzymatic activity on physiological glucose concentrations.

N,N-Dimethyl-5-((2-methyl-6-((5-methylpyrazin-2-yl)carbamoyl)benzofuran-4-yl)oxy)pyrimidine-2-carboxamide (PF-04937319, Figure 1) is a partial activator of GK, which has advanced to Phase 2 clinical trials for the treatment of T2DM (Pfefferkorn et al., 2011). The preclinical pharmacokinetics of PF-04937319 in animals were characterized by low to moderate plasma clearance and elimination half-lives, respectively (Pfefferkorn et al., 2011). The predicted hepatic clearance using liver microsomes and hepatocytes from rat and dog were found to be in good agreement with the *in vivo* blood clearance values in these species implying that the clearance mechanism of PF-04937319 involves metabolism. Renal and/or biliary excretion in rats following intravenous administration of PF-04937319 was minimal (< 3% of the administered dose) (Pfefferkorn et al., 2011), which further supports the hypothesis. First-in-human pharmacokinetics and tolerability studies in T2DM patients have been recently conducted with PF-04937319, which provided us with an opportunity to examine circulating human metabolites. Metabolite scouting studies using steady state plasma samples from the 100 mg and 300 mg oral doses of PF-04937319 led to the characterization of an *N*-demethylated metabolite (*N*-methyl-5-((2-methyl-6-((5-methylpyrazin-2-yl)carbamoyl)benzofuran-4-yl)oxy)pyrimidine-2-carboxamide, M1). Because the exposure of M1 was significantly greater than 10% of the total drug-related material based on UV response, it was proposed to be a major human metabolite of PF-04937319. On the basis of both the U.S. Food and Drug Administration Metabolites in Safety Testing (MIST) guidance and the later published 2009 ICH guidance M3 (R2) (U.S. Food and Drug Administration, 2008; European Medicines Agency, 2009), the coverage of M1 in toxicology species needed to be assessed. The current article presents a summary of the human

metabolite scouting efforts and efforts towards the examination of systemic exposure coverage in animals and characterization of the on- and off-target pharmacology profile of M1.

Materials and Methods

General Chemicals. PF-04937319 and M1 (chemical purity > 99% by HPLC and NMR) were synthesized at Pfizer Worldwide Research and Development (Groton, CT). The synthesis of PF-04937319 has been previously published (Pfefferkorn et al., 2011). A synthetic scheme for the preparation of M1 is depicted in the supplementary materials and methods section (supplementary figure S1). Monobasic and dibasic potassium phosphate buffer, magnesium chloride, and reduced β -nicotinamide adenine dinucleotide 2'-phosphate (NADPH) were purchased from Sigma-Aldrich (St. Louis, MO). Recombinant CYPs (rCYPs) 1A2, 2C19, 2C9, 2D6, 2E1, 3A4, and 3A5 were purchased from Panvera (Carlsbad, CA), whereas, rCYP2B6, 2C8, and pooled male and female human liver microsomes (HLM, $n = 50$ donors) were purchased from BD Gentest (Woburn, MA). Cryopreserved rat, dog, and human hepatocytes were obtained from Celsis (Chicago, IL).

***In Vitro* Metabolism in Cryopreserved Hepatocytes.** Stock solutions of PF-04937319 were prepared in 10% dimethyl sulfoxide (DMSO) and 90% acetonitrile. The final concentration of DMSO and acetonitrile in the incubation mixtures were 0.1% and 0.9%, respectively. Williams E media was prepared by adding 26 mM sodium carbonate and 50 mM HEPES, followed by 0.2 μ m filtration then 30 min of CO₂ bubbling at 37 °C. This media was used for thawing and suspension of hepatocytes. Rat, dog, and human hepatocytes were suspended at 0.5 million viable cells per ml Williams E medium in 24-well polystyrene plates and prewarmed at 37 °C for

30 min. Incubations were initiated with the addition of PF-04937319 (final concentration in incubation = 10 μ M) and were conducted at 37 °C for 240 min, 75% relative humidity, and 5% CO₂. The total incubation volume was 1 ml per well. Incubations were terminated by the addition of ice-cold acetonitrile (4 ml) and centrifuged (3000 x g, 15 min). The supernatants were dried under a steady stream of nitrogen, reconstituted with 25% aqueous acetonitrile (250 μ l), and analyzed via LC-MS/MS for metabolite formation.

M1 formation in rCYPs and HLM. Initial incubations were conducted in individual rCYPs or HLM to determine the time and protein concentration associated with the linear range of M1 formation. Linearity was assessed at 0.1–1.5 mg/ml protein from 10–40 min with 60 μ M of PF-04937319. rCYPs and liver microsomes were diluted to the desired concentrations in 100 mM potassium phosphate buffer (pH 7.4) and NADPH, and MgCl₂ were added to final concentrations of 1.3 and 1.0 mM, respectively. As such, PF-04937319 is very slowly metabolized in HLM, which is reflected in its minimal metabolic turnover ($t_{1/2}$ > 120 min) in NADPH-supplemented HLM (Pfefferkorn et al., 2011). The 60 μ M concentration was simply chosen to allow facile detection and quantitation of the M1 metabolite in these preliminary studies. For control incubations, a stock of HLM was placed in a 90 °C water bath for 15 min to heat-inactivate enzymes. Aliquots of diluted matrices were placed in tubes in a 37 °C dry heat bath and pre-warmed for 5 min. To initiate the reaction, PF-04937319, prepared at 100-times the final concentration (6 mM) in 10% DMSO and 90% acetonitrile, was added to the incubations (final volume = 0.4 ml). Incubations were conducted in duplicate. At each time point, 100 μ l of incubation mixture was removed and transferred to a plate containing 200 μ l of acetonitrile with 200 ng/ml terfenadine (molecular weight = 472) as internal standard. Standards of M1 were

prepared in acetonitrile and combined with 100 μ l heat-inactivated HLM in potassium phosphate buffer and 200 μ l acetonitrile with internal standard. 100 μ l of blank acetonitrile was added to each sample to match the dilution of the standards. Plates were vortexed and centrifuged (10 min, 2000 x g). 150 μ l of supernatant was removed and combined with 150 μ l water containing 0.2% formic acid. Samples were analyzed by LC-MS/MS to determine M1 concentration in each sample. M1 formation rates were calculated by dividing M1 concentration by reaction time and enzyme concentration.

Enzyme kinetics studies were conducted with the enzymes that produced appreciable amounts of M1: HLM, rCYP1A2, rCYP2C9, rCYP2C19, rCYP2D6, rCYP3A4, and rCYP3A5. From the linearity data, a protein concentration and time were selected that were within the linear range of M1 formation: HLM 0.5 mg/ml, 30 min; rCYP1A2 0.5 mg/ml (53 pmol/ml), 30 min; rCYP2C9 0.25 mg/ml (61 pmol/ml), 20 min; rCYP2C19 0.25 mg/ml (28 pmol/ml), 20 min; rCYP2D6 0.5 mg/ml (59 pmol/ml), 30 min; rCYP3A4 0.25 mg/ml (22 pmol/ml), 20 min; and rCYP3A5 0.5 mg/ml (39 pmol/ml), 30 min. Incubations were carried out as described above, in triplicate, containing PF-04937319 from 1–300 μ M. Rate of product formation was plotted versus substrate concentration. If product formation was saturated, the GraphPad PRISM (LaJolla, CA) Michaelis-Menten model was used to calculate constants K_m and V_{max} ; V_{max} was divided by K_m to calculate intrinsic clearance (CL_{int}). Otherwise, the slope of the initial reaction rate was calculated using Microsoft Excel (Redmond, WA) which is equivalent to CL_{int} . To determine contribution by each enzyme, CL_{int} was corrected for pmol CYP per mg protein, fraction unbound in incubation (HLM $f_{u,inc}$ used as a surrogate for $f_{u,inc}$ in rCYPs) and CL_{int} -derived intersystem extrapolation factors (ISEF) as previously described in the literature

(Stringer et al., 2009; Chen et al., 2011). rCYP CL_{int} values were summed and the fraction of total CL_{int} attributed to each rCYP was converted to % contribution.

Plasma Protein Binding. The binding of PF-04937319 and M1 to rat (5 males/5 females), dog (5 males/5 females), and human (3 males and 3 females) plasma proteins was determined using disposable Rapid Equilibrium Dialysis device with pre-packed inserts (ThermoScientific, West Palm Beach, FL). Stock solutions of PF-04937319 were prepared in water/acetonitrile (50/50, v/v), whereas those of M1 were prepared in DMSO. Plasma samples were prepared by mixing PF-04937319 or M1 to produce final incubation concentrations of 0.55 and 5.0 μ M for PF-04937319 and 2 μ M for M1. Aliquots (220 μ l; $n = 4$) of spiked plasma were added to the red side of the equilibrium dialysis device inserts, followed by the addition of buffer (350 μ l; $n = 4$) to the white side. The device was covered with a gas permeable membrane and agitated on an orbital shaker at approximately 450 rpm within a humidified 75% RH 5% CO₂ incubator operating at 37 °C for 4 h. Control plasma samples ($t = 0$; 15 μ l; $n = 2$) were prepared from the remaining spiked plasma solution. Each sample was matrix matched with blank buffer (45 μ l). The samples were precipitated with an acetonitrile solution (120 μ l; containing 5% DMSO and 200 ng/ml of a proprietary internal standard (molecular weight = 687). Plasma (15 μ l) and buffer (45 μ l) were sampled from each insert. The samples were matrix matched with appropriate blank matrix (plasma samples with 45 μ l of buffer and buffer samples with 15 μ l of plasma). All samples for analysis were prepared in a 96-well plate, centrifuged (3000 x g , 10 min, 25 °C), and the supernatants were analyzed by LC-MS/MS. Nonspecific binding of PF-04937319 and M1 to the equilibrium dialysis device was minimal based on control equilibrium dialysis experiments

replacing plasma with buffer. The percentage of PF-04937319 or M1 bound to plasma proteins was calculated as $100 - [(concentration\ of\ analyte\ in\ buffer / concentration\ of\ analyte\ in\ plasma) \times 100]$.

Metabolite Scouting in Humans. The study was conducted in compliance with the International Conference on Harmonization Good Clinical Practices guidelines, the ethical principles that have their origin in the Declaration of Helsinki, and the U.S. Food and Drug Administration regulations for informed consent and protection of subject rights. The clinical study design with PF-04937319 incorporated randomized, placebo- controlled multiple oral doses of 10, 30, 50, 100, and 300 mg QD for 14 days in patients with T2DM (NCT01272804). The study enrolled 12 patients (9 on actives, 3 on placebos) in 5 separate cohorts (total of approximately 60 patients). After an overnight fast, patients received PF-04937319 (10 and/or 100 mg strength tablet) and venous blood samples from each subject were collected predose (10 ml) and at 0.5, 1.5, 3.0, 5.0, 8.0, 12, and 16 h postdose (3 ml/time point) on Days 1 and 14, respectively, for examining steady state pharmacokinetics of PF-04937319. Blood samples were also collected from each subject at 2.0, 6.0, and 12 h postdose (2 ml/time point) on Days 1 and 14 for metabolite scouting efforts. Drug administration on Days 1 and 14 was following an overnight fast of at least 8 h, whereas PF-04937319 was administered with a morning meal for the remaining 12 days (Days 2–13). Blood samples were collected in heparinized tubes. Within 30 min after collection, the blood samples were centrifuged at approximately 1700 x g for ~ 10 min at 4 °C to generate plasma. All samples were stored at or below – 20 °C until analysis. Plasma for metabolite scouting was obtained from subjects in the cohort dosed with 100 mg and 300 mg of PF-04937319. Day 1 and Day 14 plasma samples were pooled according to the

method of Hamilton et al. (1981). An equal volume (0.5 ml) from each individual subject pool (pre- and post-dose) was combined to make a multi-subject pool for both Day 1 and Day 14 samples. Each pool was diluted with 12 ml of ice-cold acetonitrile with 0.1% formic acid and vortexed for 2–4 min. The samples were subsequently sonicated for 5 min, centrifuged (2000 x *g* for 10 min), and the supernatants were transferred to clean tubes and evaporated to dryness *in vacuo* under a steady nitrogen stream. The dried samples were then reconstituted in 300 µl of mobile phase (10% acetonitrile, 0.1% formic acid in water) and an aliquot (50 µl) was injected on LC-MS/MS and examined for circulating metabolites.

M1 Coverage in Preclinical Species. All studies were conducted in accordance with the United States Food and Drug Administration Good Laboratory Practice Regulations, Title 21 of the United States Code of Federal Regulations Part 58. All procedures in the protocol were in compliance with applicable animal welfare acts and were approved by the local Institutional Animal Care and Use Committee. PF-04937319 was formulated in 1.25% (w/v) hydropropyl cellulose-SL and 0.05% (w/v) docusate sodium sulfate in reverse osmosis water.

Rats. Male (0.3–0.4 kg) and female (0.2–0.3 kg) Sprague Dawley rats (4/sex/dose) were administered PF-04937319 by oral gavage once daily at doses of 50, 250, and 1000 mg/kg (males) and 10, 50, and 1000 mg/kg (females) for 3 months (at least 91 consecutive days). Blood samples were collected on Days 1 and 90 at 0.5, 2.0, 7.0, and 24 h postdose. Blood (approximately 0.5 ml) was collected from the jugular vein into tubes containing K2EDTA and centrifuged within 1 h of collection. Plasma was harvested and stored at -10 to -30 °C.

Dog. Male and female purebred Beagles (11–12 months old, 8.7–11.7 kg males, 6.0–8.7 kg, females) were administered PF-04937319 (n=3/sex/dose) by oral gavage at doses of 5.0, 50 or 250/125/100 mg/kg/day for 3 months. During the study, a reduction in dose from 250 mg/kg/day to 125 mg/kg/day occurred after 1 week of dosing, due to hypoglycemia observed in some dogs. On day 17, the glucose level was still critical, and this led to a further lowering of the dose from 125 mg/kg/day to 100 mg/kg/day preceded by 4 days of dosing holiday. Serial blood samples were collected from all animals at the following time points: 0.5, 2, 7, 12, and 24 hours after dosing on study Days 1 and 91 for toxicokinetic measurements of PF-04937319 and M1. Blood (approximately 1.0 ml) was collected into tubes containing K2EDTA and centrifuged within 1 h of collection. Plasma was harvested and stored at -10 to -30 °C.

LC-MS/MS Analysis for Quantitation of PF-04937319 and M1. Pharmacokinetics and toxicokinetics assessment for PF-04937319 and M1 from clinical and 3-month preclinical (rat and dog) toxicology studies was conducted using a validated LC-MS/MS method (Pfizer data on file). For *in vitro* studies, samples were analyzed directly using a AB Sciex (Framingham, MA) API4000 QTrap triple quadrupole LC-MS/MS with Turbo IonSpray Source, CTC Leap autosampler (Leap Technology, Carrboro, NC), and Shimadzu LC-20AD HPLC system (Columbia, MD). Samples (10 µl) were injected onto a Halo 2.7 µm C18 3.0 x 30 mm column (Advanced Materials Technology, Wilmington, DE) and analytes were eluted using a binary gradient at a flow rate of 1.2 ml/min. Mobile phase A consisted of 0.1% formic acid in water and mobile phase B 0.1% formic acid in acetonitrile. Initial conditions (10% B) were held for 0.3 min and then increased to 45% B over 0.3 min, then to 75% B over 1.4 min, increased to 90% B over 0.1 min, held for 0.2 min, and returned to initial conditions for column re-

equilibration. Analytes were detected using multiple reaction monitoring mode for the mass-to-charge (m/z) transitions 433.2 \rightarrow 324.4 (PF-04937319), 419.2 \rightarrow 310.1 (M1), and 472.5 \rightarrow 436.4 (terfenadine, internal standard). M1 standards were fit by least-squares regression of their areas to a weighted linear equation, from which the unknown concentrations were calculated. The dynamic range was 1-1000 nM.

LC-MS/MS Conditions for Metabolite Identification. Qualitative assessment of the metabolism of PF-04937319 in hepatocytes was conducted using a Thermo Finnegan Surveyor photodiode array plus detector, Thermo Acela pump and a Thermo Acela Autosampler (ThermoFinnigan, West Palm Beach, FL). Chromatography was performed on a Phenomenex Hydro RP C18 (4.6 mm x 150 mm, 3.5 μ m) column (Phenomenex, Torrance, CA). The mobile phase composed of 5 mM ammonium formate buffer with 0.1% formic acid (pH=3) (solvent A) and acetonitrile (solvent B) at a flow rate of 1 ml/min. The binary gradient was as follows: solvent A to solvent B ratio was held at 95:5 (v/v) for 3 min and then adjusted to 55:45 (v/v) from 0 to 35 min, 30:70 (v/v) from 35 to 45 min, and 5:95 (v/v) from 45 to 52 min where it was held for 3 min and then returned to 95:5 (v/v) for 6 min before next analytical run. Identification of the metabolites was performed on a Thermo Orbitrap mass spectrometer operating in positive ion electrospray mode. The spray potential was 4 V and heated capillary was at 275 °C. Xcalibur software version 2.0 was used to control the HPLC-MS system. Full scan measurements from 50–1000 amu were collected at 15,000 resolution, with two data-dependent acquisition scans of the most intense ion in scan event 1 and 2, respectively. Product ion spectra were acquired at a normalized collision energy of 65 eV with an isolation width of 2 amu. The dynamic exclusion function was used with a 1 min exclusion duration after 3 successive product

ion scans with an early exclusion if the precursor ion falls below a signal to noise ratio of 20. Metabolites from hepatocyte incubations were identified in the full-scan mode (from m/z 100 to 850) by comparing $t = 0$ samples with $t = 240$ min samples or through comparison with synthetic standard(s), and structural information was generated from the collision-induced dissociation (CID) spectra of the protonated molecular ions (MH^+).

Pharmacokinetic/Toxicokinetic Parameters. Pharmacokinetic parameters were determined using noncompartmental analysis. Maximum plasma concentrations (C_{max}) of PF-04937319 or M1 (following administration of PF-04937319) in plasma were estimated directly from the experimental data, with T_{max} defined as the time of first occurrence of C_{max} . The area under the plasma concentration–time curve (AUC) from $t=0$ to 24 or 48 h was estimated using the linear trapezoidal rule.

Results

***In Vitro* Metabolic Profile.** Figure 2 depicts HPLC-UV chromatograms of cryopreserved rat (panel A), dog (panel B), and human (panel C) hepatocyte incubations conducted with PF-04937319 (10 μ M) at 37 °C for 240 min. A total of 16 metabolites were detected in hepatocytes from preclinical species and human. There were no human-unique metabolites of PF-04937319; metabolites derived from human hepatocytes were observed in corresponding matrices from rat and/or dog. Table 1 indicates the retention time (t_R) and molecular weight (MH^+) for PF-04937319 and its corresponding metabolites obtained in hepatocyte incubations. Structural assignments for key diagnostic fragment ions in the CID spectra of PF-04937319 and its metabolites are also displayed in Table 1.

Metabolite Identification. PF-04937319 ($t_R = 22.3$ min) displayed an exact mass of 433.1619 (MH^+). Product ion scans MS^2 (Supplemental Figure S2, panel A) of PF-04937319 yielded fragment ions with m/z 324.0979 and 342.1084. The fragment ion at m/z 324.0979 represented amide bond cleavage and loss of the 5-methylpyrazin-2-amine functionality. The fragment ion at m/z 342.1084 was consistent with a gas phase addition of water to the m/z 324.0979 fragment. MS^3 product ion scans (Supplemental Figure S2, panel B) of the $m/z = 324.0979$ yielded additional fragment ions at m/z 296.1029, 281.0555, 253.0607, 225.0657. The origins of these ions are depicted in Table 1.

Metabolite M1 ($t_R = 20.4$ min) displayed an exact mass of 419.1462 (MH^+), which was 14 Da lower than the molecular weight of PF-04937319. M1 was observed in hepatocytes from rat, dog, and human. The CID spectrum of M1 (Supplemental Figure S3) contained a diagnostic fragment ion at m/z 310.0822, which was 14 Da lower than the fragment ion at m/z 324.0979 in the CID spectrum of PF-04937319. M1 was identified as the *N*-demethylated metabolite of PF-04937319 (i.e., *N*-methyl-5-((2-methyl-6-((5-methylpyrazin-2-yl)carbamoyl)benzofuran-4-yl)oxy)pyrimidine-2-carboxamide), with demethylation occurring on the *N,N*-dimethylcarboxamido motif. The t_R and mass spectral characteristics of M1 formed in liver microsomes and hepatocytes were identical to the ones discerned with an authentic standard (data not shown). M1 was the major metabolite of PF-04937319 in human hepatocytes.

Metabolite M2 ($t_R = 19.7$ min) displayed an exact mass of 449.1567 (MH^+), which was 16 Da greater than parent drug. M2 was observed in hepatocytes from rat and human. M2 underwent in-source fragmentation to yield fragment ions at m/z 431.1465 and 419.1467 (Supplemental Figure S4). The ion at m/z 419.1467 and the corresponding fragment ions at m/z 388.1041,

360.1091, 281.0557, which were obtained from the MS² fragmentation of the m/z 419.1467 (Supplemental Figure S4) suggested that hydroxylation occurred on the *N,N*-dimethylcarboxamide motif in PF-04937319. M2 was tentatively identified as the carbinolamide metabolite of PF-04937319 (i.e., *N*-(hydroxymethyl)-*N*-methyl-5-(2-methyl-6-((5-methylpyrazin-2-yl)carbamoyl)benzofuran-4-yloxy)pyrimidine-2-carboxamide.

Metabolite M3 ($t_R = 18.9$ min) displayed an exact mass of 342.1084 (MH⁺). M3 was observed in hepatocytes from rat, dog, and human. The MS² product ion spectrum contained a diagnostic fragment ion at m/z 324.0980, which gave rise to additional ions at m/z 296.1029, 281.0557, 253.0607, and 225.0659 in the MS³ product ion spectra. M3 was identified as 4-(2-(dimethylcarbamoyl)pyrimidin-5-yloxy)-2-methylbenzofuran-6-carboxylic acid, which is derived from hydrolytic cleavage across the amide bond in PF-04937319.

Metabolite M4 ($t_R = 18.25$ min) displayed an exact mass of 328.0929 (MH⁺), which is 14 Da lower than the molecular weight of M3. M4 was observed in rat hepatocytes. The MS² product ion spectrum of M4 yielded a diagnostic fragment ion at m/z 310.822, which is 14 Da less than m/z 324.0980 fragment found in M3. M4 was identified as 2-methyl-4-(2-(methylcarbamoyl)pyrimidin-5-yloxy)benzofuran-6-carboxylic acid, which is derived from an *N*-demethylation in M3.

Metabolite M5 ($t_R = 18.1$ min) displayed an exact mass of 449.1568 (MH⁺), which was 16 Da greater than PF-04937319. M5 was observed in hepatocytes from rat, dog, and human. The MS² product ion spectrum yielded diagnostic fragment ions at m/z 431.1462 and 324.0980. The ion at m/z 324.0980 (also found in the CID spectrum of PF-04937319) suggested that the site of

monohydroxylation was on the methylpyrazine motif. The fragment ion at m/z 431.1462, which corresponded to loss of a water molecule, suggested that hydroxylation occurred on the benzylic position (i.e., the methyl group) rather than on the pyrazinyl ring. M5 was tentatively assigned as 5-(((6-((5-(hydroxymethyl)pyrazin-2-yl)carbamoyl)-2-methylbenzofuran-4-yl)oxy)-*N,N*-dimethylpyrimidine-2-carboxamide).

Metabolite M6 ($t_R = 17.8$ min) displayed an exact mass of 384.1302 (MH^+) and fragment ions at m/z 367.1040 and 341.1246 in the MS^2 product ion spectrum (Supplemental Figure S5). M6 was observed in hepatocytes from dog and human. The fragment ion at m/z 341.1246 suggested that M6 was derived from a modification to the methylpyrazine motif. The fragment ion at m/z 367.1040, which represented a loss of ammonia suggested that an oxidative scission of the pyrazine ring had occurred to yield a stable urea metabolite (i.e., 1-(4-(2-(dimethylcarbamoyl)pyrimidin-5-yl)oxy)-2-methylbenzofuran-6-carbonyl)urea). A plausible mechanism that could account for the formation of M6 from PF-04937319 is shown in Figure 3A.

Metabolite M7 ($t_R = 17.6$ min) displayed an exact mass of 358.1040 (MH^+). Metabolite M7 was only observed in rat hepatocytes. M7 underwent in-source fragmentation to yield product ions m/z 340.0932 and m/z 328.0932. The m/z 340.0932 fragment, which is 16 Da higher than the m/z 324.0980 fragment ion in M3, suggested M7 was a monohydroxylated metabolite of M3. The fragment ions at m/z 297.0506 and 269.0559 in the MS^2 product ion spectrum of the m/z 340.0932 fragment suggested modification of the *N,N*-dimethylcarboxamido motif. M7 was tentatively identified as the carbinolamide metabolite of M3 (i.e., 4-(2-

((hydroxymethyl)(methyl)carbamoyl)pyrimidin-5-yl)oxy)-2-methylbenzofuran-6-carboxylic acid).

Metabolite M8 ($t_R = 16.8$ min) displayed an exact mass of 449.1568 (MH^+). Metabolite M8 was observed in hepatocytes from rat, dog, and human. The MS^2 product ion spectrum of M8 contained fragment ions at m/z 431.1463, 358.1035 and 340.0928 (Supplemental Figure S6). MS^3 product ion spectrum of the m/z 340.0928 fragment yielded several additional fragment ions at m/z 312.0977, 297.0504 and 168.0766, which were consistent with monohydroxylation on the methylbenzofuranyl motif. The m/z 431.1463 fragment in the MS^2 spectrum, representing a facile loss of water, strongly suggested that hydroxylation was occurring specifically on the 2-methyl position of the benzofuranyl motif. M8 was tentatively identified as 5-((2-(hydroxymethyl)-6-((5-methylpyrazin-2-yl)carbamoyl)benzofuran-4-yl)oxy)-*N,N*-dimethylpyrimidine-2-carboxamide. M8 was the major metabolite of PF-04937319 in dog hepatocytes.

Metabolite M9 ($t_R = 16.6$ min) displayed an exact mass of 341.1244 (MH^+). Metabolite M9 was observed in dog and human hepatocytes. The MS^2 product ion spectrum of M9 (Supplemental Figure S7) contained a diagnostic fragment ion at m/z 324.0982, which is also found in the CID spectrum of M3. The 1 mass unit difference between M3 and M9 (oxygen vs nitrogen based on exact mass) suggested M9 was an amide derivative (i.e., 5-((6-carbamoyl-2-methylbenzofuran-4-yl)oxy)-*N,N*-dimethylpyrimidine-2-carboxamide). A plausible mechanism that accounts for the formation of M9 from **1** is shown in Figure 3B.

Metabolite M10 ($t_R = 16.3$ min) displayed an exact mass of 435.1411 (MH^+). Metabolite M10 was observed in rat hepatocytes. The MS^2 product ion spectrum of M10 displayed diagnostic fragment ions at m/z 417.1306 and 326.0773. The fragment ions at m/z 417.1306 (which represented the loss of a water molecule) and m/z 326.0773 (2 mass units greater the fragment ion at m/z 324) were consistent with hydroxylation of the 2-methylbenzofuranyl motif and *N*-demethylation. MS^3 product ion spectra of the m/z 326.0773 ion yielded additional fragment ions at m/z 298.0820, 154.0608, and 136.0502 all of which were consistent with the proposed modification. M10 was tentatively identified as 5-((2-(hydroxymethyl)-6-((5-methylpyrazin-2-yl)carbamoyl)benzofuran-4-yl)oxy)-*N*-methylpyrimidine-2-carboxamide. M10 was the major metabolite of PF-04937319 in rat hepatocytes.

Metabolite M11 ($t_R = 15.8$ min) displayed an exact mass of 465.1518 (MH^+). Metabolite M11 was observed in rat hepatocytes. M11 underwent in-source fragmentation to yield fragment ions at m/z 447.1408 and 435.1410. The MS^2 product ion spectra of the m/z 447.1408 ion yielded diagnostic fragment ions at m/z 404.0989, 376.1041, 338.0771, and 297.0507, which were consistent with hydroxylation of the 2-methylbenzofuran and the *N,N*-dimethylcarboxamide groups. M11 was tentatively identified as a *N*-(hydroxymethyl)-5-((2-(hydroxymethyl)-6-((5-methylpyrazin-2-yl)carbamoyl)benzofuran-4-yl)oxy)-*N*-methylpyrimidine-2-carboxamide.

Metabolite M12 ($t_R = 15.3$ min) displayed an exact mass of 421.1624 (MH^+), which was 12 Da lower than the molecular weight of PF-04937319. Metabolite M12 was observed in dog and human hepatocytes. The MS^2 product ion spectrum of M12 (Supplemental Figure S8) contained fragment ions at m/z 403.1514, 342.1086, 324.0979 and 298.1189. The ions at m/z 324.0979 and 298.1189 suggested a modification on the methylpyrazine group. Based on exact mass, a

structure involving oxidative constriction of the pyrazine ring with loss of a carbon atom was proposed for M12 (i.e., *N,N*-dimethyl-5-((2-methyl-6-((2-methyl-2H-imidazol-4-yl)carbamoyl)benzofuran-4-yl)oxy)pyrimidine-2-carboxamide), and a plausible mechanism for its formation is shown in Figure 3C.

Metabolite M13 ($t_R = 15.2$ min) displayed an exact mass of 451.1359 (MH^+). Metabolite M13 was observed in rat hepatocytes. M13 underwent in-source collision to yield product ions m/z 433.1255 and 421.1254. The MS^2 product ion spectrum of the m/z 433.1255 fragment showed diagnostic fragment ions at m/z 404.0987 and 324.0616, which were consistent with hydroxylations on the 2-methyl benzofuranyl and the *N*-methylcarboxamido groups in metabolite M1. M13 was tentatively identified as *N*-(hydroxymethyl)-5-((2-(hydroxymethyl)-6-((5-methylpyrazin-2-yl)carbamoyl)benzofuran-4-yl)oxy)pyrimidine-2-carboxamide.

Metabolite M14 ($t_R = 15.0$ min) displayed an exact mass of 518.1405 (MH^+). Metabolite M14 was observed in hepatocytes from rat, dog, and human. The MS^2 product spectrum of M14 showed a characteristic glucuronide loss of 176 Da to yield product ion m/z 342.1084, which is the molecular mass of M3. Therefore, M14 was identified as the acyl glucuronide conjugate of M3 (i.e., 5-((4-(2-(dimethylcarbamoyl)pyrimidin-5-yloxy)-2-methylbenzofuran-6-carbonyl)oxy)-3,4,6-trihydroxy-tetrahydro-2H-pyran-2-carboxylic acid).

Metabolite M15 ($t_R = 14.5$ min) displayed an exact mass of 358.1033 (MH^+). M15 was observed only in rat hepatocytes. The MS^2 product spectrum contained diagnostic fragment ions at m/z 340.0928, 315.0614, 297.0505, which were consistent with monohydroxylation of the 2-

methylbenzofuran motif in the hydrolytic product M3. M15 was tentatively identified as 4-(2-(dimethylcarbamoyl)pyrimidin-5-yloxy)-2-(hydroxymethyl)benzofuran-6-carboxylic acid.

Metabolite M16 ($t_R = 14.0$ min) displayed an exact mass of 344.0873 (MH^+). M16 was observed only in rat hepatocytes. The MS^2 product ion spectrum of M16 contained diagnostic fragment ions at m/z 326.0773 and 297.0519, which were consistent with *N*-demethylation in M15. M16 was tentatively identified as 2-(hydroxymethyl)-4-(2-(methylcarbamoyl)pyrimidin-5-yloxy)-benzofuran-6-carboxylic acid.

M1 Formation Rates in HLM and rCYPs. PF-04937319 (60 μM) and NADPH (1.3 mM) were incubated for 10–40 min with HLM (0.1–1.5 mg/ml), heat-inactivated HLM, or rCYPs, which included rCYP1A2, rCYP2B6, rCYP2C8, rCYP2C9, rCYP2C19, rCYP2D6, rCYP2E1, rCYP3A4, and rCYP3A5 isozymes, to determine linearity of M1 formation. Linear protein concentrations and incubation times were selected for each enzyme and enzyme kinetics were determined at PF-04937319 concentrations of 1.0–300 μM . K_m and V_{max} or initial reaction rate were used to generate CL_{int} , which was in turn used to calculate percent contribution to metabolism by each rCYP. ISEF-corrected M1 formation rates were highest in rCYP3A4, rCYP2C9, and rCYP2C19 incubations (Table 2). The total CL_{int} in rCYP (0.62 $ml \cdot min^{-1} \cdot mg^{-1}$) was slightly higher than the CL_{int} noted in HLM (0.23 $ml \cdot min^{-1} \cdot mg^{-1}$).

Circulating Metabolites of PF-04937319 in Humans. Circulating metabolites of PF-04937319 in human were qualitatively examined in the 100 mg and 300 mg dose groups from the multiple dose study. Plasma samples were pooled according to the method of Hamilton et al. (1981) and metabolic profile in steady state samples (Day 14) was compared with Day 1 samples. A total of

eight metabolites were detected in human plasma from both dose groups. Figure 4 shows a representative HPLC-UV ($\lambda = 310$ nm) trace of pooled plasma from humans dosed with 300 mg of PF-04937319. Of the eight metabolites detected, only two, M1 and a minor metabolite designated as M3a were observable in the UV trace ($\lambda = 310$ nm), the remainder of the metabolites (M3, M4, M5, M8, M10, and M14 shown in Table 1) were detectable at trace levels by MS only. The major components observed in human plasma were M1 and unchanged parent drug. Based on UV integration, PF-04937319 and M1, respectively, accounted for 40% and 50% of circulating drug related material at Day 1 and 31% and 65% of drug related material at Day 14. Metabolite M3a ($t_R = 18.4$ min) displayed a MH^+ at 435.1411, which was 2 Da higher than PF-04937319 (see Table 1). The exact mass of M3a was consistent with *N*-demethylation and hydroxylation of PF-04937319. The product ion spectrum of M3a contained diagnostic fragment ions at m/z 417.1302 and 405.1304, which suggested that both metabolic steps occurred on the *N,N*-dimethylamide portion in PF-04937319. M3a has been tentatively identified as the *N*-desmethyl carbinolamide metabolite of PF-04937319 (i.e., *N*-(hydroxymethyl)-5-((2-methyl-6-((5-methylpyrazin-2-yl)carbamoyl)benzofuran-4-yl)oxy)pyrimidine-2-carboxamide). Overall, these data suggest that M1 had accumulated to a significant extent at steady state (Day 14) compared to Day 1.

Comparison of M1 Concentrations in Animals and Humans. Because M1 was present at levels greater than 10% of circulating drug related material, it became necessary to qualify the metabolite in preclinical species as per the MIST guidance. Consequently, an authentic standard of M1 was synthesized, followed by a quantitative analysis of M1 in the plasma samples from the multiple dose human study and the 3-month rat and dog toxicity studies as a representative

case. Table 3 lists the pharmacokinetic parameters of M1 in humans administered with 100 mg and 300 mg of PF-04937319 once daily for 14 days. For the purposes of comparison, the toxicokinetic parameters of M1 (on Days 1 and 90/91) in rats and dogs at the no-observed-adverse-effect level (NOAEL) doses of 1000 mg/kg (male rats)/50 mg/kg (female rats) and 5 mg/kg (male and female dogs) are also shown. Figures 5, 6, and 7 illustrate representative mean total plasma concentration versus time profile for PF-04937319 and M1 in humans (Days 1 and 14 at the 300 mg dose of PF-04937319), rats (Days 1 and 90 at the 50 mg/kg (female) and 1000 mg/kg (male) doses of PF-04937319), and dogs (Days 1 and 90 at the 5 mg/kg doses of PF-04937319), respectively.

Systemic exposures of M1 were assessed by comparison of C_{max} and/or AUC on Day 1 and steady state (i.e., Day 14 for human and Day 90 or 91 for rat and dog). Both total and free plasma concentrations were examined in the analysis. In humans, systemic exposure to M1 increased in a dose-dependent fashion (100–300 mg) with 1.9–2.8-fold accumulation of M1 over the period of 14 days. The estimated half-life ($t_{1/2}$) of M1 in humans dosed with PF-04937319 was ~ 23 h for the two dose strengths. Compared with the steady state levels of M1 observed in humans at the 100 mg and 300 mg dose groups of PF-04937319, the NOAEL dose of 5 mg/kg in male or female dogs revealed considerably lower circulating levels of M1 (total or free) at steady state. PF-04937319 demonstrated a gender difference in rat pharmacokinetics; female rats exhibited higher systemic exposure than male rats due to a lower plasma clearance, leading to differences in NOAEL between male and female animals. Examination of total and free steady state exposures (Day 91) of M1 in female rats dosed with 50 mg/kg of PF-04937319 also did not reveal sufficient coverage of the steady state M1 levels (total or free) observed in humans.

Steady state M1 exposure in humans at the 100 mg dose group of PF-04937319 was covered in terms of total C_{\max} (~7.7x) and total AUC (~3.6x) in male rats dosed with 1000 mg/kg of PF-04937319 for 90 days. Steady state M1 exposure in humans at the 300 mg dose group of PF-04937319 was covered on the basis of total C_{\max} (~ 1.8x) and AUC (0.8x) in male rats dosed with 1000 mg/kg of PF-04937319 for 90 days.

Plasma Protein Binding. The extent of *in vitro* binding of PF-04937319 and M1 to plasma proteins was evaluated by equilibrium dialysis in rat, dog, and human plasma. The mean (\pm S.D.) unbound fraction of PF-04937319 at concentrations of 0.55 and 5.5 μM were 0.24 ± 0.02 and 0.24 ± 0.01 (rat), 0.37 ± 0.02 and 0.39 ± 0.02 (dog), and 0.30 ± 0.02 and 0.32 ± 0.02 (human). The mean unbound fraction of M1 (2 μM , equivalent to 0.837 $\mu\text{g/ml}$) in rat, dog, and human was 0.0801, 0.192, and 0.142, respectively. These results indicate that M1 has slightly higher plasma protein binding than PF-04937319. Both PF-04937319 and M1 were stable in rat, dog, and human plasma for 4 h at 37 °C at the concentrations used in the plasma free fraction determination.

Discussion

The current article discloses our initial findings on MIST studies with the glucokinase activator PF-04937319 that were conducted during Phase 1 clinical studies. Examination of human pharmacokinetics following 14 days of daily administration of PF-04937319 (10–300 mg) revealed mean terminal $t_{1/2}$ values ranging from 6.3–8.5 h, which also were in reasonable agreement with the predicted $t_{1/2}$ value using hepatic clearance values from liver microsomes and/or hepatocytes and volume of distribution from allometric scaling of animal data. Consistent

with the observations in preclinical species, less than 1% of the oral dose was excreted unchanged in urine.

Qualitative examination of the *in vitro* metabolic fate in rat, dog, and human hepatocytes revealed that PF-04937319 was metabolized via oxidative and hydrolytic pathways (Figure 8). Although there were no human unique metabolites, differences were noted with regards to the biotransformation profile of PF-04937319 across preclinical species and human. *N*-demethylation to M1 was the major route of metabolism in human hepatocytes, while M10, derived from a hydroxylation of the 2-methylbenzofuran group in M1, was the major metabolite in rat hepatocytes. In the case of dog, monohydroxylation at the 2-methylbenzofuran group in PF-04937319 resulting in M8 was the dominant metabolic fate. Of much interest was the formation of the metabolites M6, M9, and M12 that were derived from pyrazine ring scission. The proposed structures of M6, M9, and M12 shown in Table 1 are consistent with the observed molecular weight and fragmentation pattern. Postulated mechanisms leading to the formation of M6, M9, and M12 are depicted in Figure 3. Pyrazine ring oxidation to epoxide **1** and its subsequent ring opened form **2** were proposed as common intermediates in the formation of M6 and M12, respectively (Figure 3, pathways A and C). In the case of M6, addition of water on the pyrazine ring in **2** would lead to the diol **3**, followed by ring scission to the dihydrooxazole intermediate **4**. The formation of M6 from **4** can occur via a two step process involving hydrolysis across the carboximidoamide motif in **4** to **5** followed by elimination of 4-methyloxazole and water. The formation of M12 can be envisioned from a pyrazine ring scission in **2** to a 2*H*-imidazole-carbaldehyde intermediate **6**. The hemiacetal form of the 2*H*-imidazole-carbaldehyde derivative (i.e., **7**) could then spontaneously lose carbon dioxide and

lead to M12 (Figure 3C). In the case of M9, a two-electron oxidation on the 2-amino-5-methylpyrazine motif could lead to the corresponding imine-methide intermediate **8** followed by hydrolysis to the primary carboxamide metabolite M9 via the intermediate carbinolamine **9** (Figure 3B). The mechanisms depicted in Figure 3 are purely speculative, and will require additional mechanistic studies as further proof for the proposed pathways. A pragmatic starting point involving the isolation, purification and NMR characterization of M7, M9, and M12 to obtain unequivocal proof for the proposed structures is currently ongoing in our laboratories.

Metabolite characterization in early development phase has been the major focus of MIST discussions and although the strategic approaches and methodologies may vary, there is a clear consensus that an assessment of circulating metabolite exposure across species at steady state to underwrite safety is a critical component of this stage (Aurell Holmberg et al., 2014; Haglund et al., 2014; Nedderman et al., 2011; Yu et al., 2010; Leclercq et al., 2009; Luffer-Atlas, 2008). The availability of steady state plasma samples from the 14 day study on PF-04937319 in T2DM patients were an appropriate starting point towards MIST studies. Plasma samples from the 100 mg and 300 mg dose groups were chosen for the analysis, since they represented an efficacious dose range based on glucose lowering effects observed in the T2DM patients (Pfizer data on file). The major components in human plasma were unchanged parent drug and M1, an observation that was consistent with the *in vitro* metabolic profile in human hepatocytes and previous literature (Dalvie et al, 2009). Because M1 accounted for 65% of the drug related material on Day 14, its synthesis was triggered and the authentic standard was used for quantitative comparison of steady state exposures in plasma from human and the 3-month safety studies in rats and dogs at the NOAEL. The $t_{1/2}$ of M1 (~ 23 h) was significantly longer than the

$t_{1/2}$ of the parent compound (~ 6.3–8.5 h), and as a result, the systemic exposure of M1 was higher than the exposure of the parent compound at steady state at both the 100 and 300 mg doses. In contrast, the circulating levels of M1 were very low in beagle dogs and female rats. Steady state human exposure of M1 at the 100 mg and the 300 mg dose group, however, was covered in terms of total C_{max} (~7.7x and 1.8x for the 100 mg and 300 mg, doses, respectively) in male rats. Likewise, male rats provided a 3.6x and 0.8x AUC coverage for M1 at the human doses of 100 and 300 mg, respectively. Because AUC differences of ≥ 2 -fold are generally considered to be meaningful in toxicokinetic evaluations (International Conference on Harmonisation, 2012), our present data indicate that M1 is toxicologically qualified at this time. Of much interest was the identification of the minor circulating metabolite M3a, which was tentatively assigned as a carbinolamide derivative of M1. The formation of M3a can potentially occur via a CYP mediated *N*-demethylation of PF-04937319 to M1 followed by a two-electron oxidation of M1 to an iminium species, which can generate M3a upon hydration of the iminium bond. Surprisingly, liver microsomal or hepatocyte incubations of PF-04937319 in rat, dog and human failed to generate M3a. It is possible that M3a is a very minor metabolic fate of PF-04937319, and the qualitative *in vitro* metabolism studies using unlabeled PF-04937319 may not be sensitive enough to detect its presence. *In vitro* studies are in progress to examine whether the formation of M3a proceeds via the M1 metabolite. Greater granularity in terms of total body burden of M1 and M3a will be necessary in subsequent mass balance studies in rats and human, especially for M3a, which can be labeled as human unique (even though it constitutes only ~4% of total drug related material). Likewise, further studies will be conducted as necessary to maintain adequate exposure of at least one animal species to metabolite M1 and particularly

M3a. This will ultimately be dependent on the clinically efficacious doses of PF-04937319 utilized in future trials, and the corresponding NOAEL in longer term (> 3 months) toxicity studies.

The availability of an authentic standard of M1 also facilitated efforts into CYP phenotyping. Examination of the rates of formation of M1 in incubations of PF-04937319 in a panel of recombinant human CYP isozymes revealed that M1 is mainly formed by CYP3A4, CYP2C9, and CYP2C19. Comparison of the plasma protein binding of PF-04937319 and M1 in the preclinical species of toxicological evaluation (rat and dog) and human revealed that M1 was ~ 3-, 2-, and 2-fold more bound to plasma proteins in rat, dog, and human, respectively. A recent drug-drug interaction (DDI) guidance from the European Medicines Agency (www.ema.europa.eu/docs/en_GB/document_library/Scientific_guideline/2012/07/WC500129606.pdf) and the draft DDI guidance from the Food and Drug Administration (www.fda.gov/downloads/Drugs/GuidanceComplianceRegulatoryInformation/Guidances/ucm292362.pdf) have proposed that metabolites present at >25% of the parent AUC and >10% of the total drug-related exposure should be investigated *in vitro* for their DDI potential. Therefore, the inhibitory potential of M1 against the major human CYP isoforms was examined and compared with the parent compound. Both PF-04937319 and M1 were devoid of competitive CYP inhibition against CYP1A2, CYP2C8, CYP2C19, CYP2D6, and CYP3A4 (IC₅₀ values > 30 μM) (Pfizer data on file). PF-04937319 and M1 were also devoid of time- and concentration-dependent inhibitory effects on CYP3A4.

Additional investigations on the on- and off-target pharmacology of M1 were also initiated. First and foremost, the pharmacologic activity of PF-04937319 and M1 was compared in the *in*

in vitro biochemical activation assay (Pfefferkorn et al. 2011), which revealed that M1 was significantly less potent as a human GK activator than the parent compound (PF-04937319: $EC_{50} = 0.17 \mu\text{M}$; M1: $EC_{50} = 4.69 \mu\text{M}$). Furthermore, at the 300 mg dose group, the steady state unbound C_{max} of M1 in humans was estimated to be $0.54 \mu\text{M}$, which is significantly lower than its *in vitro* EC_{50} value. Additional assessment of safety revealed that M1 (like the parent compound) was devoid of mutagenic responses in the *Salmonella* Ames assay (in the absence or presence of metabolic activation). Likewise, no off-target activity was discerned upon evaluation of M1 (at a concentration of $100 \mu\text{M}$) for broader pharmacological activity in a panel of receptors, ion channels and enzymes in the CEREP panel (<http://www.cerep.fr/cerep/users/pages/productservices/industrialization.asp>). In conclusion, we have described a case study on the assessment of the MIST regulatory guidance during the early development phase of a clinical candidate, and the initial pragmatic steps undertaken to de-risk/qualify a metabolite that exceeded 10% of total drug related material in humans. Insights gained in this analysis should lead to a more efficient and focused development plan for fulfilling MIST requirements with PF-04937319.

Authorship Contributions

Participated in research design: Raman Sharma, Karen Atkinson, Heather Eng, Neeta B. Amin, John Litchfield, John C. Pettersen Theunis C. Goosen, Li Di, William S. Denney, Deepak K. Dalvie, and Amit S. Kalgutkar

Conducted in vitro experiments: Raman Sharma, Karen Atkinson, Heather Eng

Conducted clinical study: Neeta Amin

Contributed new reagents or analytic tools: Raman Sharma, Esther Lee, Jeffrey A. Pfefferkorn

Performed data analysis: Raman Sharma, Karen Atkinson, Heather Eng, Neeta B. Amin, John Litchfield, John C. Pettersen, Theunis C. Goosen, Li Di, William S. Denney, Deepak K. Dalvie, and Amit S. Kalgutkar

Wrote or contributed to the writing of the manuscript: Raman Sharma, Karen Atkinson, Heather Eng, Neeta B. Amin, John Litchfield, Theunis C. Goosen, Li Di, William S. Denney, Deepak K. Dalvie, Jeffrey Pfefferkorn, and Amit S. Kalgutkar

References

- Aurell Holmberg A, Ekdahl A, and Weidolf L (2014) Systemic exposure to the metabolites of lesogaberan in humans and animals – a case study of metabolites in safety testing. *Drug Metab Dispos* 42:1016-1021.
- Chen Y, Liu L, Nguyen K, and Fretland AJ (2011) Utility of intersystem extrapolation factors in early reaction phenotyping and the quantitative extrapolation of human liver microsomal intrinsic clearance using recombinant cytochrome P450. *Drug Metab Dispos* 39:373-382.
- Coghlan M and Leighton B (2008) Glucokinase activators in diabetes management. *Expert Opin Invest Drugs* 17:145-167.
- Dalvie D, Obach RS, Kang P, Prakash C, Loi CM, Hurst S, Nedderman A, Goulet L, Smith E, Bu HZ, and Smith DA (2009) Assessment of three human in vitro systems in the generation of major human excretory and circulating metabolites. *Chem Res Toxicol* 22:357-368.
- Di L, Trapa P, Obach RS, Atkinson K, Bi YA, Wolford AC, Tan B, McDonald TS, Lai Y, Tremaine LM (2012) A novel relay method for determining low-clearance values. *Drug Metab Dispos* 40:1860-1865.
- Di L, Atkinson K, Orozco CC, Funk C, Zhang H, McDonald TS, Tan B, Lin J, Chang C, Obach RS (2013) In vitro-in vivo correlation for low clearance compounds using hepatocyte relay method. *Drug Metab Dispos* 41:2018-2023.

European Medicines Agency (2009) ICH topic M3 (R2) non-clinical safety studies for the conduct of human clinical trials and marketing authorization for pharmaceuticals. European Medicines Agency, London, UK.

Grimsby J, Sarabu R, Corbett WL, Haynes NE, Bizzarro FT, Coffey JW, Guertin KR, Hilliard DW, Kester RF, Mahaney PE, Marcus L, Qi L, Spence CL, Teng J, Magnuson MA, Chu CA, Dvorozniak MT, Matschinsky FM, and Grippo JF (2003) Allosteric activators of glucokinase: potential role in diabetes therapy. *Science* **301**:370-373.

Haglund J, Halldin MM, Brunnström A, Eklund G, Kautiainen A, Sandholm A, and Iverson SL (2014) Pragmatic approaches to determine the exposures of drug metabolites in preclinical and clinical subjects in the MIST evaluation of the clinical development phase. *Chem Res Toxicol* **27**:601-610.

Haynes NE, Corbett WL, Bizzarro FT, Guertin KR, Hilliard DW, Holland GW, Kester RF, Mahaney PE, Qi L, Spence CL, Teng J, Dvorozniak MT, Railkar A, Matschinsky FM, Grippo JF, Grimsby J, and Sarabu R (2010) Discovery, structure-activity relationships, pharmacokinetics, and efficacy of glucokinase activator (2R)-3-cyclopentyl-2-(4-methanesulfonylphenyl)-N-thiazol-2-yl-propionamide (RO0281675). *J Med Chem* **53**:3618-3615.

International Conference on Harmonisation (2012) Questions and answers (R2), ICH, Geneva, Switzerland.

Leclercq L, Cuyckens F, Mannens GS, de Vries R, Timmerman P, and Evans DC (2009) Which human metabolites have we MIST? Retrospective analysis, practical aspects, and perspectives for metabolite identification and quantification in pharmaceutical development. *Chem Res Toxicol* **22**:280-293.

Luffer-Atlas D (2008) Unique/major human metabolites: why, how, and when to test for safety in animals. *Drug Metab Rev* **40**:447-463.

Matschinsky FM and Ellerman JE (1968) Metabolism of glucose in islets of langerhans. *J Biol Chem* **243**:2730-2736.

Matschinsky FM, Glaser B and Magnuson MA (1998) Pancreatic β -cell glucokinase: closing the gap between theoretical concepts and experimental realities. *Diabetes* **47**:307-315.

Matschinsky FM, Zelent B, Doliba NM, Kaestner KH, Vanderkooi JM, Grimsby J, Berthel SJ, and Sarabu R (2011) Research and development of glucokinase activators for diabetes therapy: theoretical and practical aspects. *Handbook Exp Pharmacol* **203**:357-401.

Meininger GE, Scott R, Alba M, Shentu Y, Luo E, Amin H, Davies MJ, Kaufman KD, and Goldstein BJ (2011) Effects of MK-0941, a novel glucokinase activator, on glycemic control in insulin-treated patients with type 2 diabetes. *Diabetes Care* **34**:2560-2566.

Mithieux G (1996) Role of glucokinase and glucose-6-phosphatase in the nutritional regulation of endogenous glucose production. *Reprod Nutr Dev* **36**:357-362.

Nedderman ANR, Dear GJ, North S, Obach RS, Higton D (2011) From definition to implementation: a cross industry perspective of past, current and future MIST strategies. *Xenobiotica* **41**:605-622.

Obach RS (1999) Prediction of human clearance of twenty-nine drugs from hepatic microsomal intrinsic clearance data: An examination of in vitro half-life approach and nonspecific binding to microsomes. *Drug Metab Dispos* **27**:1350-1359.

Pfefferkorn JA, Guzman-Perez A, Oates PJ, Litchfield J, Aspnes G, Basak A., Benbow J, Berliner MA, Bian J, Choi C, Freeman-Cook K, Corbett JW, Didiuk M, Dunetz JR, Filipski KJ, Hungerford WM, Jones CS, Karki K, Ling A, Li JC, Patel L, Perreault C, Risley H, Saenz J, Song W, Tu M, Aiello R, Atkinson K, Barucci N, Beebe D, Bourassa P, Bourbonnais F, Brodeur AM, Burbey R, Chen J, D'Aquila T, Derksen DR, Haddish-Berhane N, Huang C, Landro J, Lapworth AL, MacDougall M, Perregaux D, Pettersen J, Robertson A, Tan B, Treadway JL, Liu S, Qiu X, Knafels J, Ammirati M, Song X, DaSilva-Jardine P, Liras S, Sweet L, and Rolph TP (2011) Designing glucokinase activators with reduced hypoglycemia risk: discovery of N,N-dimethyl-5-(2-methyl-6-((5-methylpyrazin-2-yl)-carbamoyl)benzofuran-4-yloxy)pyrimidine-2-carboxamide as a clinical candidate for the treatment of type 2 diabetes mellitus. *Med Chem Commun* **2**:828-839.

Pfefferkorn JA, Guzman-Perez A, Litchfield J, Aiello R, Treadway JL, Pettersen J, Minich ML, Filipski KJ, Jones CS, Tu M, Aspnes G, Risley H, Bian J, Stevens BD, Bourassa P, D'Aquila T, Baker L, Barucci N, Robertson AS, Bourbonnais F, Derksen DR, Macdougall M, Cabrera O, Chen J, Lapworth AL, Landro JA, Zavadoski WJ, Atkinson K, Haddish-Berhane N, Tan

- B, Yao L, Kosa RE, Varma MV, Feng B, Duignan DB, El-Kattan A, Murdande S, Liu S, Ammirati M, Knafels J, Dasilva-Jardine P, Sweet L, Liras S, and Rolph TP (2012) Discovery of (S)-6-(3-cyclopentyl-2-(4-(trifluoromethyl)-1H-imidazol-1-yl)propanamido)nicotinic acid as a hepatoselective glucokinase activator clinical candidate for treating type 2 diabetes mellitus. *J Med Chem* **55**:1318-1333.
- Pfefferkorn JA (2013) Strategies for the design of hepatoselective glucokinase activators to treat type 2 diabetes. *Expert Opin Drug Discov* **8**:319-330.
- Sarabu R, Berthel SJ, Kester RF, and Tilley JW (2011) Novel glucokinase activators: a patent review (2008-2010). *Expert Opin Ther Pat* **21**:13-33.
- Sarabu R, Bizzarro FT, Corbett WL, Dvorozniak MT, Geng W, Grippo JF, Haynes NE, Hutchings S, Garofalo L, Guertin KR, Hilliard DW, Kabat M, Kester RF, Ka W, Liang Z, Mahaney PE, Marcus L, Matschinsky FM, Moore D, Racha J, Radinov R, Ren Y, Qi L, Pignatello M, Spence CL, Steele T, Tengji J, and Grimsby J (2012) Discovery of piragliatin – first glucokinase activator studied in type 2 diabetes patients. *J Med Chem* **55**:7021-7036.
- Stringer RA, Strain-Damerell C, Nicklin P, and Houston JB (2009) Evaluation of recombinant cytochrome P450 enzyme as an in vitro system for metabolic clearance predictions. *Drug Metab Dispos* **37**:1025-1034.
- U.S. Food and Drug Administration (2008) Guidance for Industry: Safety Testing of Drug Metabolites. Center for Drug Evaluation and Research, U.S. Food and Drug Administration, U.S. Department of Health and Human Services, Rockville, MD.

Yu H, Bischoff D, and Tweedie D (2010) Challenges and solutions to metabolites in safety testing: Impact of the international conference on harmonization M2 (R2) guidance. *Expert Opin Drug Metab Toxicol* **6**:1539-1549.

Footnotes

The study was sponsored by Pfizer.

Figure Legends

Figure 1. Structure of partial GK activator PF-04937319.

Figure 2. HPLC-UV ($\lambda = 310$ nm) chromatograms of cyropreserved rat (panel A), dog (panel B), and human hepatocyte incubations conducted with PF-04937319 (10 μ M) at 37 °C for 240 min.

Figure 3. Postulated mechanisms for the formation of metabolite M6 (A), M9 (A and B), and M12 (C) from PF-04937319.

Figure 4. HPLC-UV ($\lambda=310$ nm) of metabolic profile of PF-04937319 (300 mg once daily for 14 days) in human plasma.

Figure 5. Mean plasma concentrations versus time profile of PF-04937319 (circles) and M1 (squares) in humans after oral administration of PF-04937319 at doses of 300 mg on Day 1 ($n=9$, closed symbols) and Day 14 ($n=7$, open symbols). Metabolite samples were pooled for analysis.

Figure 6. Mean plasma concentrations versus time profile of PF-04937319 (circles) and M1(squares) on Days 1 (closed symbols) and 90 (open symbols) in male and female rat plasma after oral administration of PF-04937319 at doses of 1000 mg/kg (males) (panel A) and 50 mg/kg (females) (panel B).

Figure 7. Mean plasma concentrations versus time profile of PF-04937319 (circles) and M1 (squares) in male dogs after oral administration of PF-04937319 at doses of 5 mg/kg on Day 1 (closed symbols) and Day 91 (open symbols).

Figure 8. Postulated biotransformation pathways of PF-04937319 in rat, dog, and/or human.

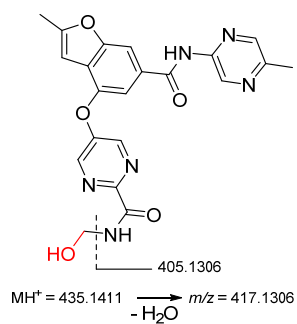
Tables

TABLE 1

Mass spectral characteristics of the metabolites of PF-04937319

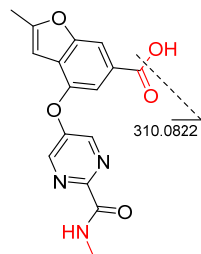
Metabolite ^a	MH ⁺	Structure	Fragment Ions
PF-04937319	433.1619		342.1084, 324.0979, 296.1029, 281.0555, 253.0607, 225.0657
M1	419.1462		310.0822, 282.0873
M2	449.1567		431.1465, 419.1467, 388.1041, 360.1091, 281.0558
M3	342.1084		324.0980, 296.1029, 281.0557, 253.0607, 225.0659

M3a 435.1411



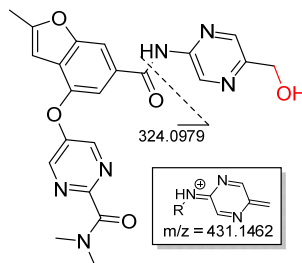
417.1302, 405.1306

M4 328.0929



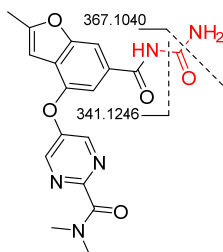
310.0822

M5 449.1568



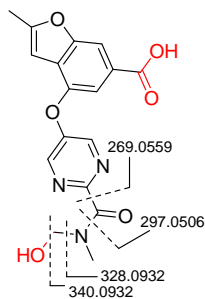
431.1462, 324.0979

M6 384.1302



367.1040, 341.1246

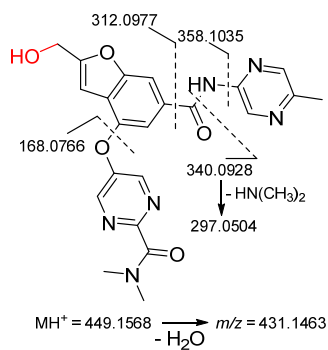
M7 358.1040



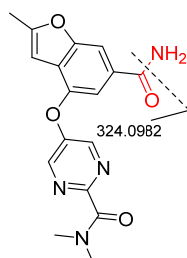
340.0932, 328.0932, 297.0506,
269.0559

DMD #60087

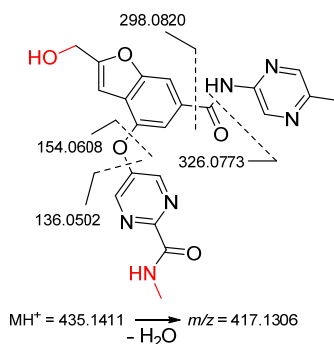
M8 449.1568 431.1463, 358.1035, 340.0928, 312.0977, 297.0504, 168.0766



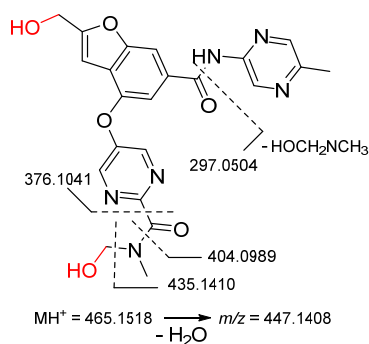
M9 341.1244 324.0982

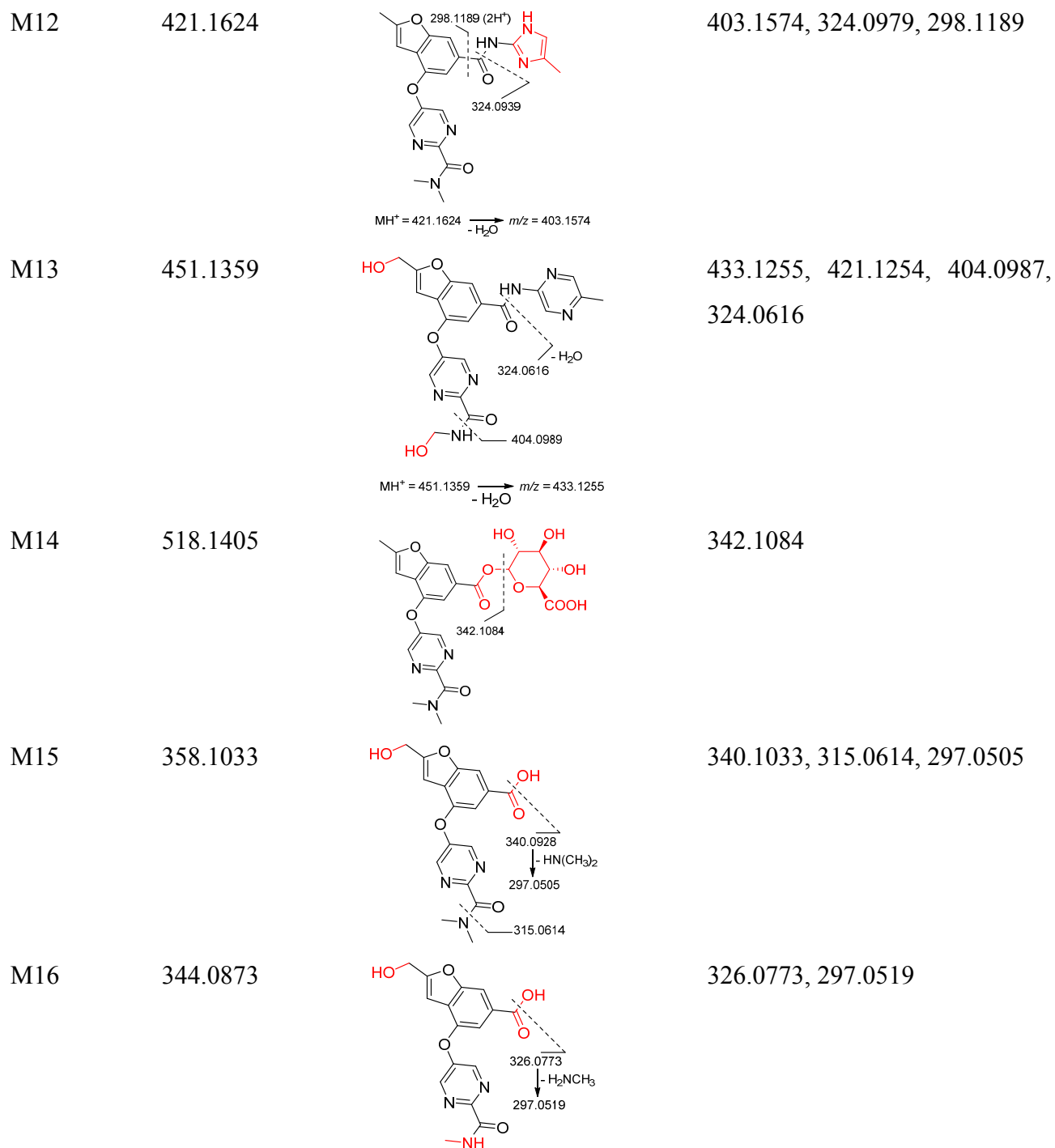


M10 435.1411 417.1306, 326.0773, 298.0820, 154.0608, 136.0502



M11 465.1518 447.1408, 435.1410, 404.0989, 376.1041, 338.0771, 297.0507





^aMetabolite numbering system is based on individual metabolite t_R on reversed phase HPLC (see Figure 2).

TABLE 2

M1 formation in rCYPs and HLM. M1 formation rates were calculated from incubations of PF-04937319 (0–300 μ M, n=3) in NADPH-supplemented rCYPs or HLM for 20–30 minutes (time associated with reaction linearity)

Enzyme Source	CL _{int} Corrected with ISEF μ l·min ⁻¹ ·mg ⁻¹ , unbound	% Contribution
HLM	0.229	-
HLM (heat-treated)	ND ^a	-
rCYP 1A2	0.0007	0.1%
rCYP 2C9	0.0680	10.9%
rCYP 2C19	0.0421	6.8%
rCYP 2D6	0.0006	0.1%
rCYP 2B6	ND	ND
rCYP 2C8	ND	ND
rCYP 2E1	ND	ND
rCYP 3A4	0.489	78.6%
rCYP 3A5	0.0214	3.4%
Sum rCYPs:	0.621	-

^aN.D. = not determined: M1 was not formed in appreciable amount.

TABLE 3
Mean pharmacokinetic parameters of M1 in humans and preclinical species of toxicological evaluation after administration of PF-04937319

Species	Gender	Dose	Day	M1			Exposure Multiples (AUC ₀₋₂₄) ^e
				C _{max} (ng/ml) ^b	T _{max} (h)	AUC ₍₀₋₂₄₎ (ng.h/ml) ^b	
Human	Mixed ^a	100 mg	1	193 (27.4)	12	3670 (521)	N.D.
Human	Mixed ^a	300 mg	1	574 (81.5)	24	10889 (1550)	N.D.
Human	Mixed ^a	100 mg	14	364 (51.7)	12	8130 (1150)	N.D.
Human	Mixed ^a	300 mg	14	1600 (227.2)	5.0	34148 (4850)	N.D.
Dog ^c	Male	5 mg/kg	1	52.3 (10.0)	2.0	441 (84.7)	0.013 (0.017)
Dog ^c	Male	5 mg/kg	91	43.9 (8.43)	2.0	419 (80.4)	0.012 (0.017)
Dog ^c	Female	5 mg/kg	1	33.8 (6.50)	2.0	332 (63.7)	0.010 (0.013)
Dog ^c	Female	5 mg/kg	91	42.1 (8.08)	2.0	385 (73.9)	0.011 (0.015)
Rat ^d	Male	1000 mg/kg	1	2800 (224)	2.0	31200 (2500)	0.92 (0.52)
Rat ^d	Male	1000 mg/kg	90	2830 (227)	7.0	45000 (3600)	1.3 (0.74)
Rat ^d	Female	50 mg/kg	1	328 (26.3)	2.0	5100 (409)	0.15 (0.08)
Rat ^d	Female	50 mg/kg	90	596 (47.7)	2.0	9974 (797)	0.29 (0.17)

^aMale and female.

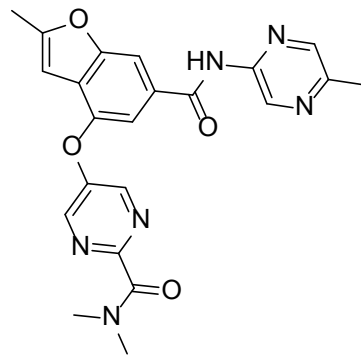
^bConcentrations of M1 depicted are *total* plasma concentrations; M1 concentrations in parenthesis reflect unbound concentrations in plasma.

^cNOAEL in the 3-month toxicity study was 5 mg/kg in male and female dogs.

^dNOAEL in the 3-month toxicity studies was 1000 mg/kg and 50 mg/kg in male and female rats, respectively.

^eExposure multiples were calculated based on Day 14 AUC₀₋₂₄ from the 300 mg dose in humans as a clinical reference.

Figure 1



PF-04937319

Figure 2

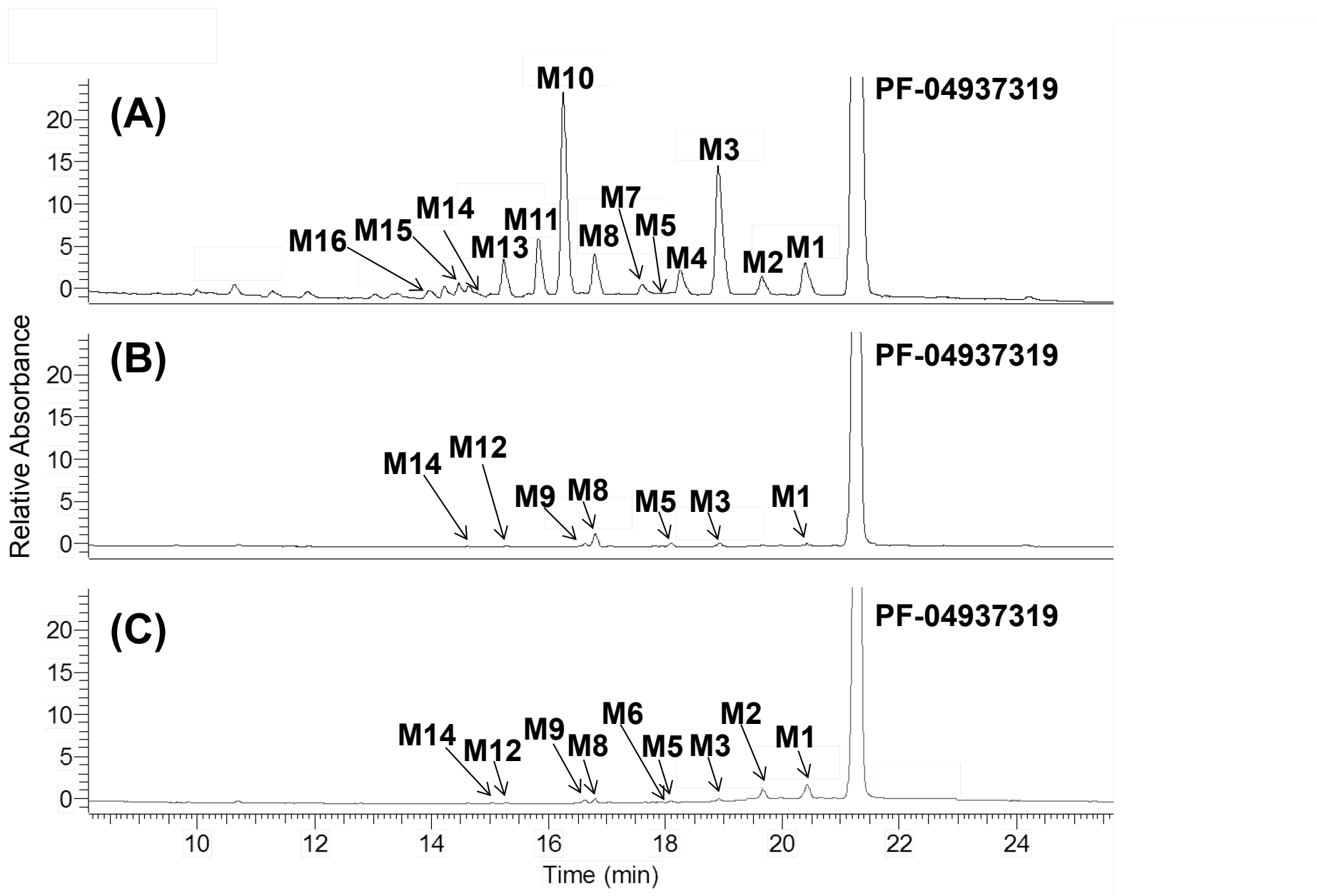
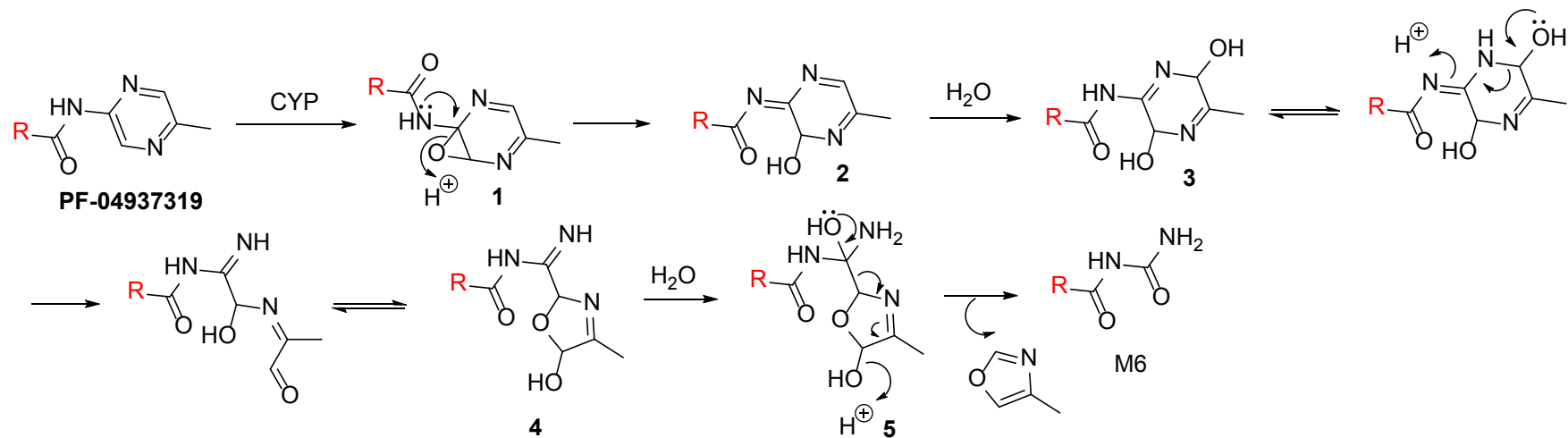
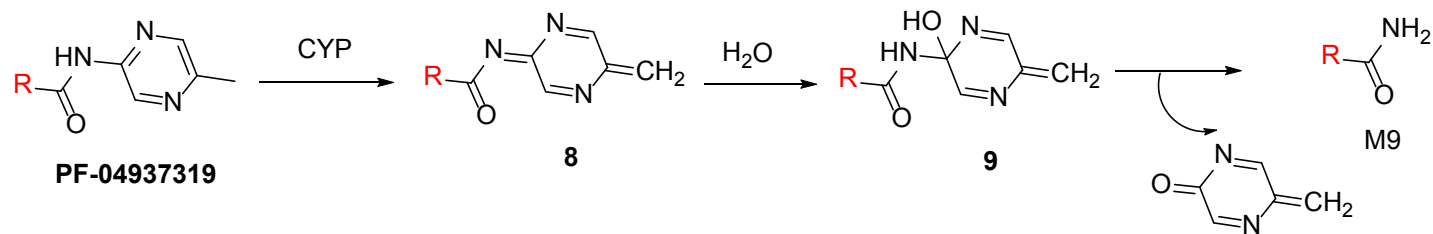


Figure 3

(A)



(B)



(C)

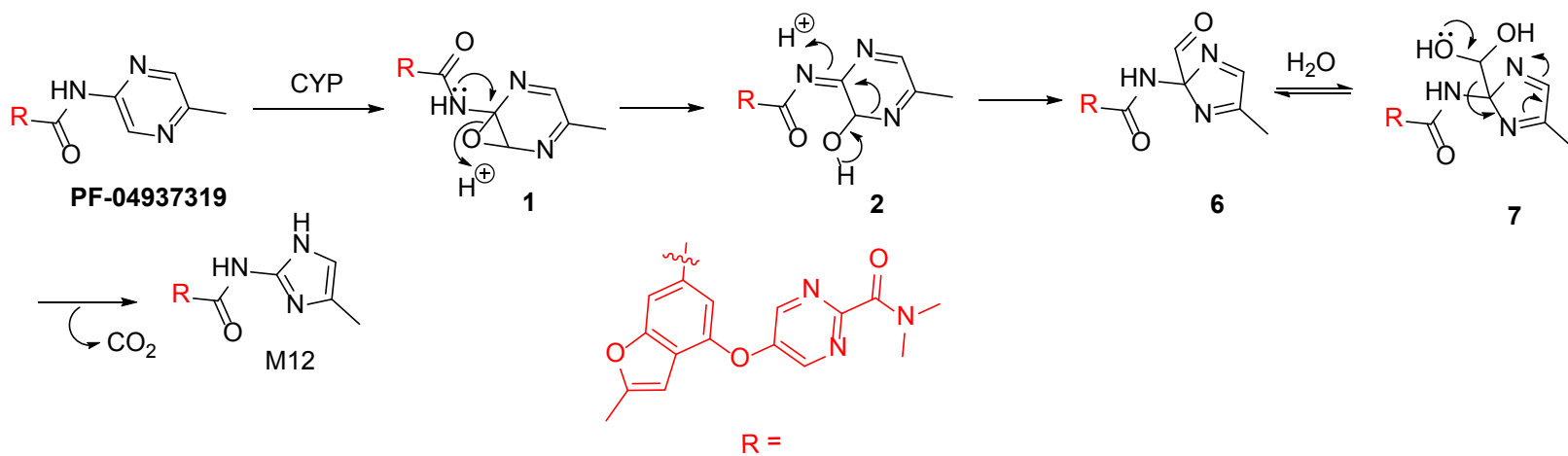


Figure 4

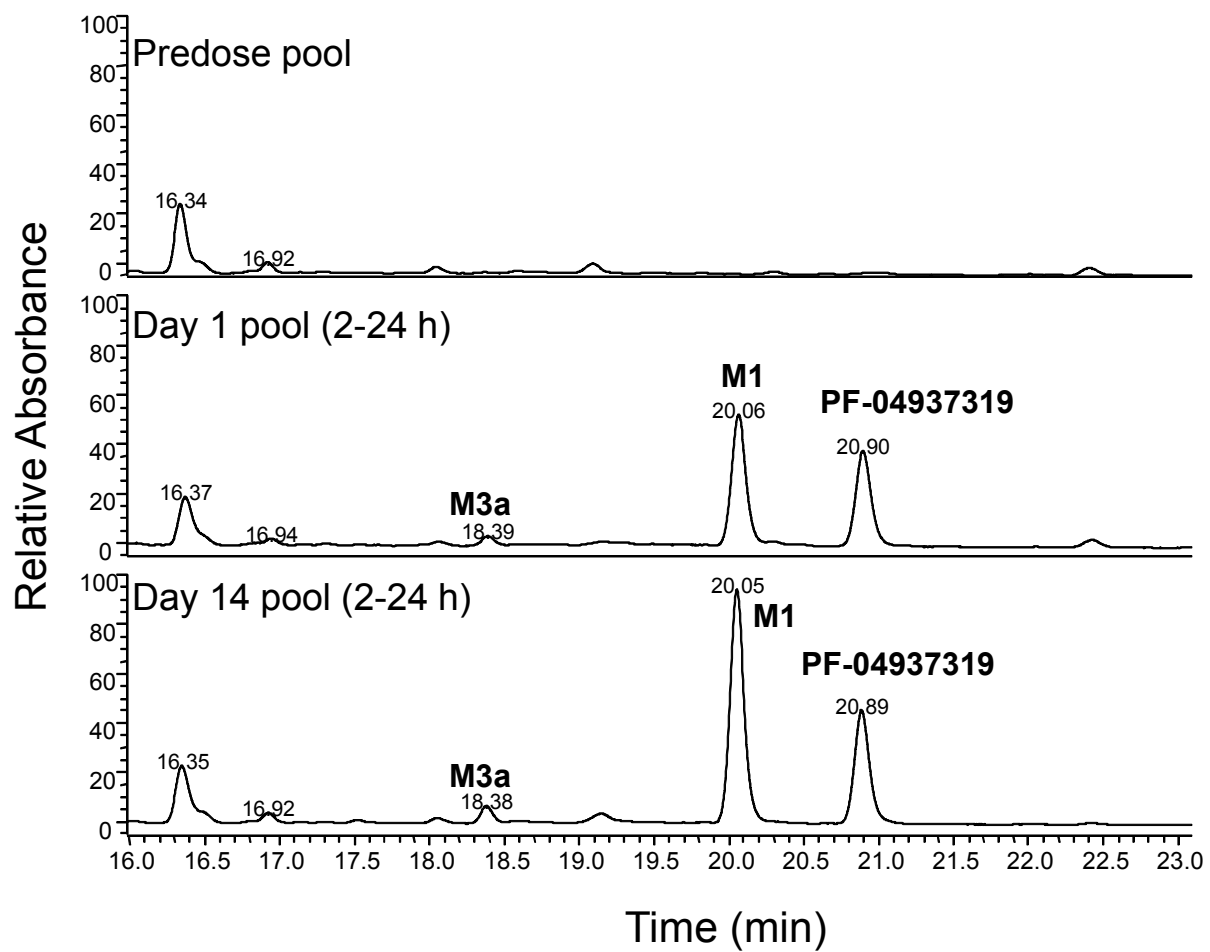


Figure 5

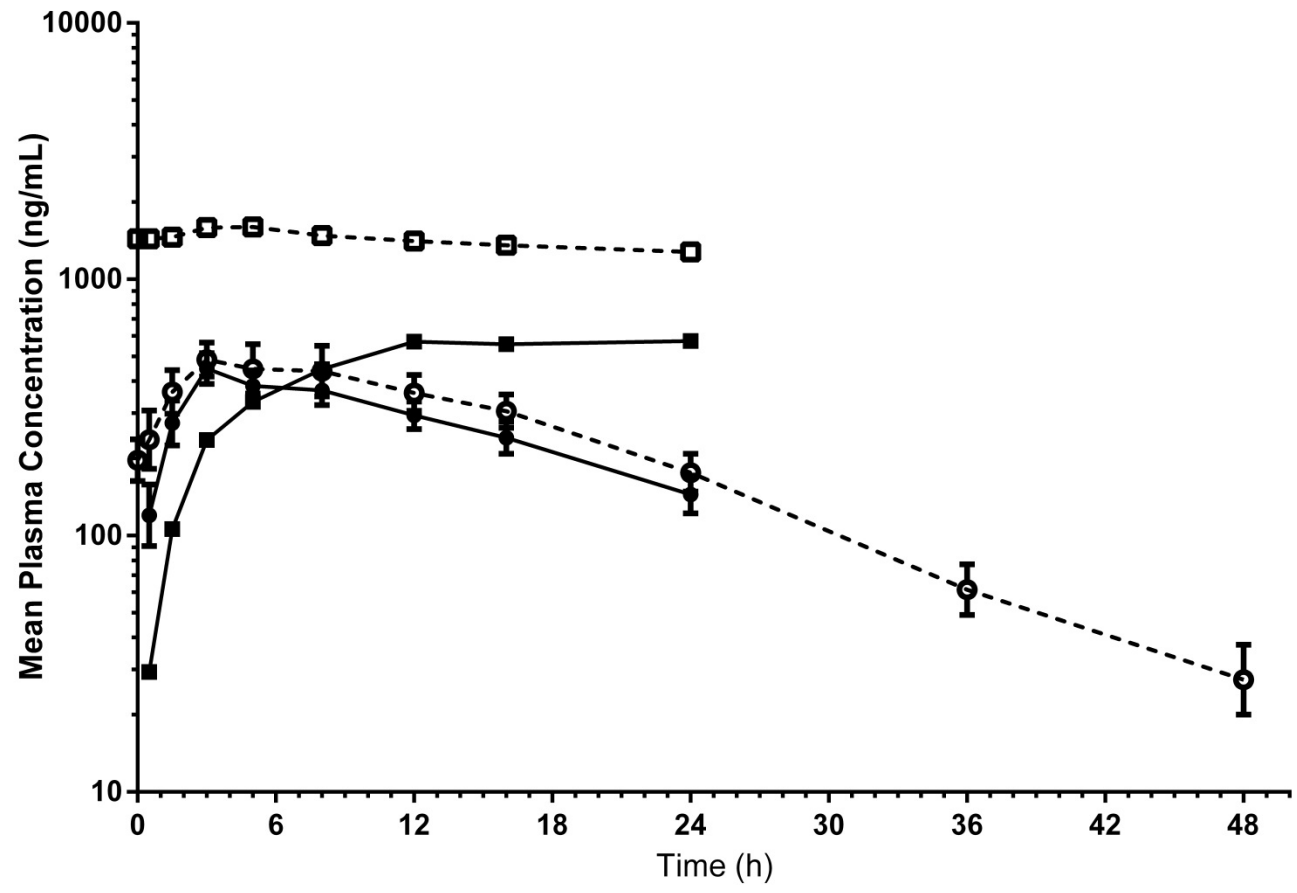


Figure 6

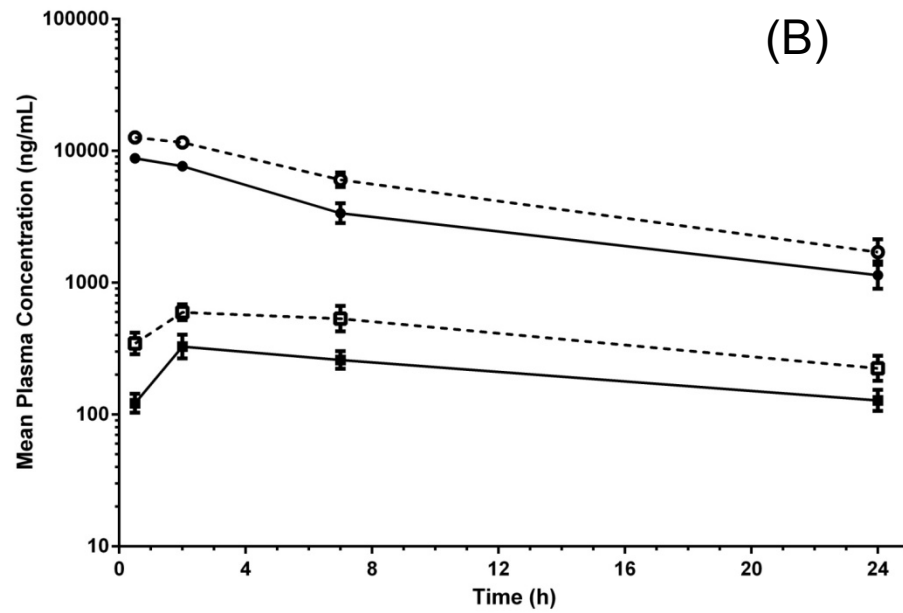
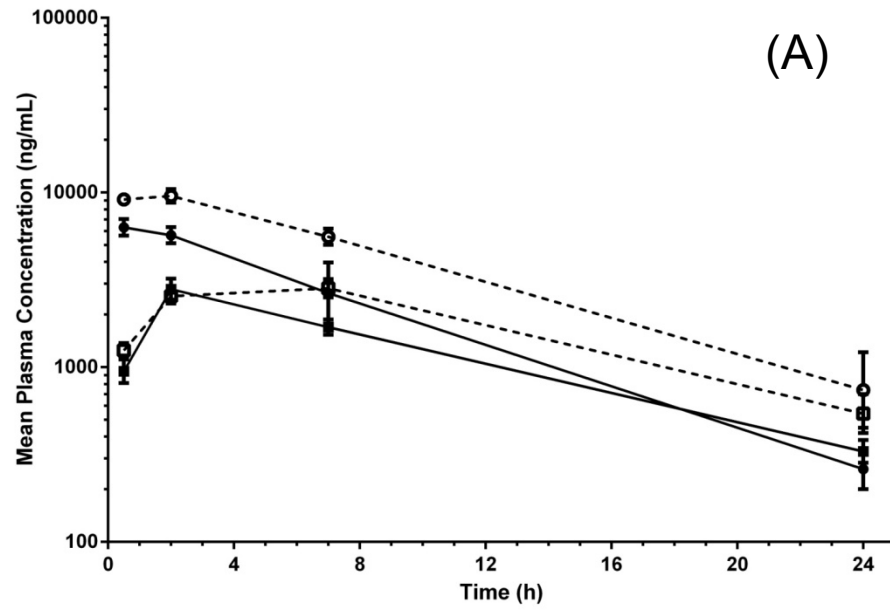


Figure 7

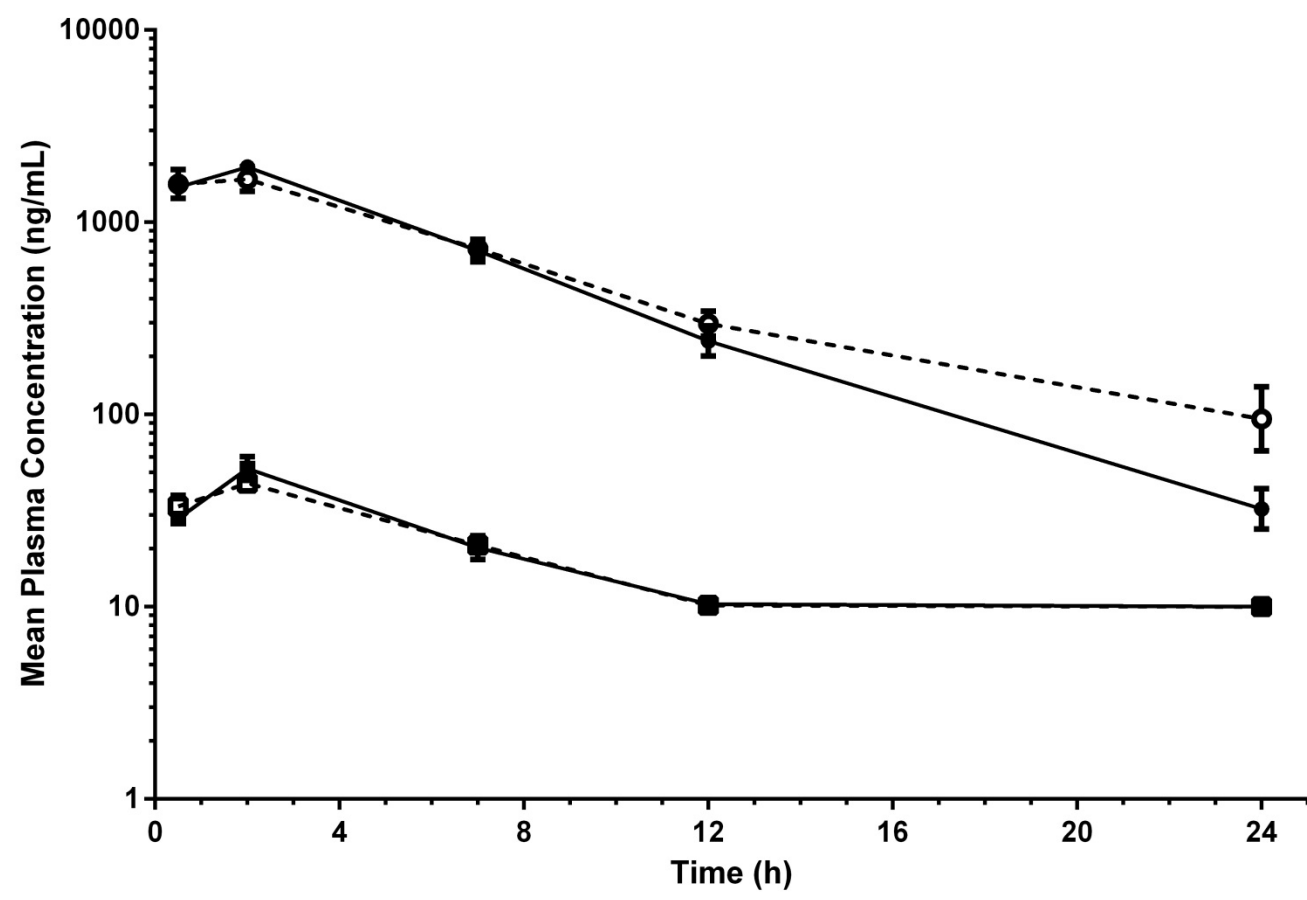


Figure 8